DOI 10.1007/s11595-017-1575-0

Effect of Niobium Addition on Hot Deformation Behaviors of Medium Carbon Ultra-high Strength Steels

YANG Xiuzhi[1,2], ZHANG Lichao[2*], SHI Yusheng[2*], YU Shengfu[2], HUA Wenlin[1]

(1.Hubei Polytechnic University, Huangshi 435003,China; 2.State Key Laboratory of Materials Processing and Die & Mould Technology, School of Materials, Science and Engineering, Huazhong University of Science and Technology, Wuhan 430074, China)

Abstract: The hot deformation behaviors of two medium carbon ultra-high strength steels with different niobium contents were investigated by using Zener-Hollmom parameter and processing map, and the effect of niobium addition on the hot deformation behavior of medium carbon steel was determined. The hot compression tests were conducted on a Gleeble-3500 thermo-mechanical simulator deformed at temperatures from 850 to 1 200 ℃ and strain rates from 0.001 to 1 s^{-1}. The processing maps of two test steels were built at a true strain of 0.7 based on dynamic materials model (DMM). There are two peak efficiency domains and two flow instability regions in both test steels. However, the peak efficiency domains of Nb-bearing steel move to higher temperature due to the inhibition of dynamic recrystallization (DRX), and the instability domains of Nb-bearing steel are enlarged due to the precipitation of Nb-containing particles during hot deformation. The optimum process parameters of Nb-bearing and Nb-free steels for industrial production were determined according to the processing map and the microstructural observation.

Key words: Nb addition; hot workability; processing map; rolling process

1 Introduction

Nb has rich reserves on the earth, and also is more effective in grain refinement compared with V and Ti. Since 1970s, the micro alloying technology by using Nb has been widely spread, thus leading to greatly improved performance and much cheaper price of metal materials[1]. By adding carbide forming elements and nitride forming elements, such as Nb, vanadium (V), titanium (Ti), molybdenum (Mo) and boron (B), in steel, the physical and chemical properties of steels can be obviously improved through the dissolution and precipitation mechanism of the compounds. According to Refs. [2-4], the compounds of NbN, NbCN and NbC can be formed in steel by the reaction between Nb and C, N. Their solubility product formula is shown as follows:

$$\lg([Nb]\cdot[M])=A-B/T \quad (1)$$

where M shows the solubility of C, N or (C, N); *A* amd B show the constants greater than zero. The carbide and nitride containing Nb are pinned at the grain boundaries in the rolling process, and the pinning force is greater than the driving force of recrystallization at that temperature, thus preventing the growth of grain, and the "pinning" effect can reach 1 100 ℃. H. Chinna, H.Norderg and R.P.Smith calculated the free energy of nitride and carbide formed by Ti, V, Nb in the austenite[4]. Dong Tao[5] summarized the precipitation strengthening potential of Ti, V, Nb during co-grid precipitation and pointed out that the dispersion strengthening effect of Nb is more effective than that of Ti and V. In the research of high Cr die steel, S.Wilms and G.Zwik[6] showed that Nb has a low solubility, which has unconspicuous effect of second hardening, but the niobium carbide can precipitate from the austenite, which helps to control the grain growth of austenite, refine the grain and improve the hardening temperature. Refs.[7, 8]show that in the hot rolling technology, the delayed recrystallization effect of Nb during deformation of austenite can obtain grain refinement, and relations of the Nb microalloyed steel strengthening and toughening were summarized. Pickering shows that the grain refinement

(Received: Oct. 20, 2015; Accepted: Nov. 4, 2016)

YANG Xiuzhi (杨秀芝) : Assoc. Prof.; Ph D; E-mail: yangliushuzhi@163.com

*Corresponding author: ZHANG Lichao(张李超): Assoc. Prof.; Ph D; E-mail: 10959439@qq.com; SHI Yusheng (史玉升): Prof.; Ph D; E-mail: shiyusheng@hust.edu.cn

Supported by the National 863 Program of China (No.2015AA042505), Hubei Department of Education Youth Program (No.Q20123001), Hubei Province Natural Science Foundation (No.2014 cfb177), Wuhan Huaxia Fine Blanking Technology Co., LTD Program (No.YYYY2014-015)

of Nb can provide metal materials with high strength and toughness simultaneously. The Nippon Steel (Japanese) developed high temperature austenitic stainless steel named YUS304N[9,10] by adding niobium and nitrogen in grade 304 steel, and compared with the original 304 steel, the weldability, strength and fatigue resistance of YUS304N were improved. At the same time, in Japan by way of adding Nb or Nb+V to SAE9260 (the original automobile spring steel), utilizing the strengthening effect of grain refinement and precipitation, the spring damper was improved, its yield strength was about 100 MPa higher than the original SAE9260 steel, and thus the material weight was reduced by about 25%. N.TSUJII[12,13] *et al* study the effect of Nb on the high temperature and low cycle fatigue behavior of H11 steel, the results show that the hardness of H11M steel after tempering is still maintained at 48HRC. In addition, S.Akiyama[6] et al developed Nb-containing ferritic stainless steel "NAR-FC-3", which was developed on the basis of original SUS430 and SUS434 by adding Nb. It was found that the surface quality, pitting resistance and formability and wrinkle resistance were much better than that of SUS430, SUS434 and 304 steel. By niobium application, the corrosion resistance in high temperature alloy can be improved, and the welding performance, metallurgical quality, anti-crack property and resistance to hydrogen sulfide corrosion in pipeline steel can be improved; the wear resistance, the strength and toughness in cast iron and cast steel can be improved. Niobium micro alloying technology is widely used in various fields of iron and steel materials, which plays a very important role in the development of the national economy[12].

The medium-carbon steels with ultra-high strength, which are regarded as the technical challenge in the field of seamless tube manufacturing, are the key materials for the an exploitation of ultra-deep oil/gas wells. In order to achieve an excellent combination of strength and impact toughness for the safety application of ultra-deep oil/gas well, proper chemical compositions, appropriate hot rolling process and fitting heating treatment are the key factors in the whole manufacturing process of seamless tube. In general, seamless tubes were prepared by sequential processes of melting in an electric furnace, continuous casting with argon shielding, reheating-piecing-hot rolling-stretching into a tube and then quenching and tempering at proper temperature and time. Piecing and hot rolling is the main process for the manufacture of seamless tube, and it will affect the final mechanical properties of the seamless tube. The effects of martensite morphology, tempering temperature and tempering time on the mechanical properties have been studied in previous studies[14-16]. But in previous studies, there was little discussion focusing on the hot deformation behaviors of medium-carbon steels with ultra-high strength.

Nb microalloyed medium carbon steel was designed by adding 0.03% Nb to a original Nb-free steel with appropriate reduction of carbon and vanadium content. Interestingly, even though the carbon content of Nb-bearing steel decreases, both strength and impact toughness were improved under the same quenching and tempering treatment compared with Nb-free steel. The strengthening effect of Nb addition was obvious in the medium carbon steel. It is well known that amongst all the microalloying elements, Nb is the most effective one retarding austenite recrystallization by means of the solute drag effects of solution Nb or by pinning effect of strain induced precipitation[17-19]. In previous studies[20-22], the effects of Nb on recrystallization behavior, precipitation hardening and phase transformation were extensively studied. But there existed little work determining the influence of Nb on the hot deformation behavior by using processing map.

The hot working behavior of test steels can be characterized using processing map. One of the most promising methods is the DMM model developed by Prasad *et al*[23,24]. The DMM model aims to correlate the constitutive behavior with the microstructural evolution, flow instability and hot workability of a wide range of materials, and optimize the hot working process of materials. Based on the DMM model, a processing map is defined as a representation of microstructural evolution mechanisms of a given material. In a processing map, the power dissipation map represents the manner in which the power is dissipated as microstructural transition or material damage, while the instability map is developed based on the principles of irreversible thermodynamics as applied to large plastic flow suggested by Kalian Kumar[24] to predict the flow instability in the processing. In order to prevent deformation defects and refine austenite microstructures, the hot rolling process should be performed in the safety region of austenite phase where dynamic or static recrystallizaiton is the dominant microstructure modifying mechanism. With the help of processing map, the regions suited for processing were determined.

Table 1 Chemical compositions of experimental steels/wt%

Test steel	C	Si+Mn	P+S	Cr+Mo+V	Nb	Al	Ti	N/ppm
Nb-bearing	0.20	0.80	0.010	1.83	0.03	0.026	0.015	69
Nb-free	0.25	0.76	0.012	1.85	—	0.03	0.013	94

The proper piecing and hot rolling process can further improve the property of seamless tube steel and achieve a combination of ultra-high strength and toughness.

Hitherto, hot working behaviors of titanium alloy, magnesium alloy, nickel alloy and stainless steels were frequently researched[23-27] in previous studies. However, in this regard, only a few reports were conducted on the hot deformation behavior of ultra-high strength medium carbon steel and few discussions were existed to determine the effect of niobium on the hot deformation behavior using processing map. The objective of the present investigation was to study the hot deformation behavior of Nb-bearing and Nb-free steels, meanwhile to determine the effect of niobium on the hot workability of medium carbon steel with ultra-high strength by using constitutive equations and processing map.

2 Experimental

The Nb-bearing and Nb-free steels used in this work were cut from the as-rolled steels after industrial pilot. The main difference in chemical composition between two steels was that 0.03 wt% Nb was added to the Nb-free steel with appropriate reduction of the carbon and vanadium content. The chemical compositions are listed in Table 1.

A Gleeble-3500 thermo-mechanical simulator was used to test the true stress-true strain curves of uniaxial hot compression. Cylindrical specimens with a diameter of 8 mm and a height of 12 mm were used in this study. Tantalum foils of 0.10 mm thickness were inserted between the anvil and the specimen to minimize friction and ensure uniform deformation. A chromel-alumel type thermocouple was welded at the mid-height of the specimen to monitor the temperature during hot compression.

The specimens were heated to 1 200 ℃ at a heating rate of 10 ℃/s and held for 10 min to ensure that all the precipitates (carbides and nitrides) of V and Nb were completely dissolved. Then, the specimens were cooled to the deformation temperature (850 to 1 200 ℃) at a cooling rate of 5 ℃/s. After 5 seconds stabilization, the specimens were compressed by four strain rates of 0.001 to 1 s^{-1} at a true strain of 0.7. Finally, the specimens were instantly quenched to room temperature by water after the compression for the purpose of preserving the hot deformation microstructures. In order to observe the optical microstructural evolution, all specimens were sectioned along the compression axis, ground, polished and etched in a mixed solution of 2 g picric acid, 50 mL deionized water and a small amount of catalyzer at 75 ℃. Microstructural observations were carried out using an optical microscope. The linear intercept method was used to determine the mean size of austenite grain by counting more than 200 grains. Carbon extraction replicas were prepared after etched at alcohol solution containing 2% nitric acid. Then the distribution and chemical composition of the second phase precipitates were examined using a JEM-2010 high-resolution transmission electron microscope (TEM) with an energy dispersive spectrometer (EDS).

As we know, it will never eliminate the fiction completely during hot deformation even though necessary lubricating measures were taken to reduce the fiction. Consequently, it is inevitable to cause the samples barreling during hot deformation. In order to accurately reflect the flow behavior, the flow stress data could be modified by the following equation[28-30]:

$$\bar{\sigma} = \frac{\sigma}{1+(2/3\sqrt{3})m(r_0/h_0)\exp(3\varepsilon/2)} \tag{2}$$

where $\bar{\sigma}$ is the corrected flow stress, σ is the measured flow stress, ε is the measured strain, m is the friction factor, r_0 and h_0 are the initial radius and height of specimen. And the friction factor m can be determined by the following expression[31]:

$$m = \frac{(r/h)\,b}{(4\sqrt{3})-(2b/3\sqrt{3})} \tag{3}$$

where $b = \frac{\Delta r}{r}\cdot\frac{h}{\Delta h}$, $\Delta r = r_M - r_T$, $r_T = \sqrt{3\frac{h}{h_0}r_0^2 - 2r_M^2}$, $\Delta h = h_0 - h$, $r = r_0\sqrt{\frac{h_0}{h}}$, h is the height of specimen after

compression, r_M and r_T are the maximum and top radius of the specimen after deformation. After the correction of flow stress using Eqs. (2) and (3), the relation of true strain *versus* true stress was obtained.

3 Results and discussion

3.1 True strain and stress curves of two materials

The corrected flow stress curves of Nb-bearing and Nb-free steels deformed at a given strain rate and a given deformation temperature are shown in Fig.1 (a) and Fig.1 (b), respectively. As shown in Fig.1, the peak stress and peak strain increase with decrease of the deformation temperature at a given strain rate, and enhance with increase of the strain rate at a given temperature. The flow stress is sensitive to the deformation temperature and strain rate. The values of peak strain, steady state strain, peak stress, and steady state stress of Nb-added steel are higher than that of Nb-free steel under the same deformation condition. It is well known that the peak stress indicates the occurrence of dynamic recrystallizaiton. In the condition of intermediate deformation temperature and lower strain rate, the stress-strain curves of Nb-added steel go to steady-state curve without experiencing the peak stress demonstrating that there is no dynamic recrystallization taking place, whereas the Nb-free steel completes a full dynamic recrystallization process, *i e*, deformed at 950 ℃ and strain rate of 0.01 s^{-1}. The niobium addition contributes to delaying dynamic recrystallization and therefore to increasing the value of peak strain and stress[32].

3.2 Kinetic analysis

During hot plastic deformation, the effect of the temperatures and strain rate on the flow stress can be described as the Zener-Hollmom parameter as follows:

$$Z = \dot{\varepsilon}\exp(\frac{Q}{RT}) \tag{4}$$

where $\dot{\varepsilon}$ is the strain rate; Q is the activation energy for hot deformation (kJ/mol); R is the universal gas constant (8.314 J/mol·K); T is the absolute temperature (K); A, α are the material constants, which are independent of deformation temperature; n is the stress exponent.

The constitutive relationship between the flow stress and Zener-Hollmom parameter can be described in the following equation known as the classical hyperbolic-sine Arrhenius-type equation fitting for stress over a wide range[33, 34]:

$$Z = A[\sinh(\alpha\sigma)]^n \tag{5}$$

By combining Eqs.(2) and (3), the following equation can be reached:

$$\dot{\varepsilon}=A[\sinh(\alpha\sigma)]^n \cdot \exp(-\frac{Q}{RT}) \tag{6}$$

By taking the natural logarithm of both sides of (6):

$$\ln\dot{\varepsilon} + \frac{Q}{RT} = \ln A + n\ln|\sigma| \tag{7}$$

$$\ln\dot{\varepsilon} + \frac{Q}{RT} = \ln A + \beta|\sigma| \tag{8}$$

According to Eqs. (7) and (8), $n=d\ln\dot{\varepsilon}/d\ln|\sigma|$, $\beta=d\ln\dot{\varepsilon}/d|\sigma|$ and $\alpha=\beta/n$. The linear relationships of $\ln\dot{\varepsilon}-\sigma$ and $\ln\dot{\varepsilon}-\ln\sigma$ at different deformation temperatures of two test steels were fitted in Fig.2 and Fig.3 at a true strain of 0.5. The slopes of the fitted curves in Figs.2(a) and (b) represent the material constants n and β. The mean values of all slopes in

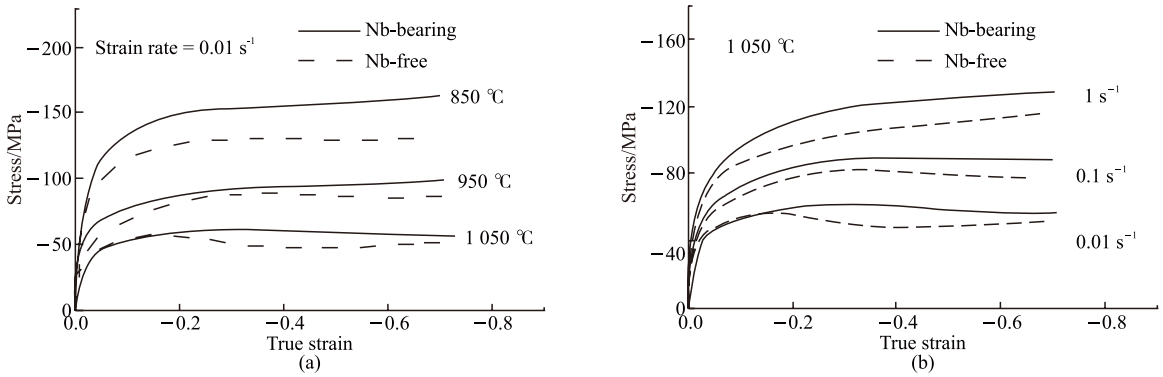

Fig.1 True stress-true strain curves for Nb-bearing and Nb-free steels at (a) different deformation temperatures and (b) strain rates

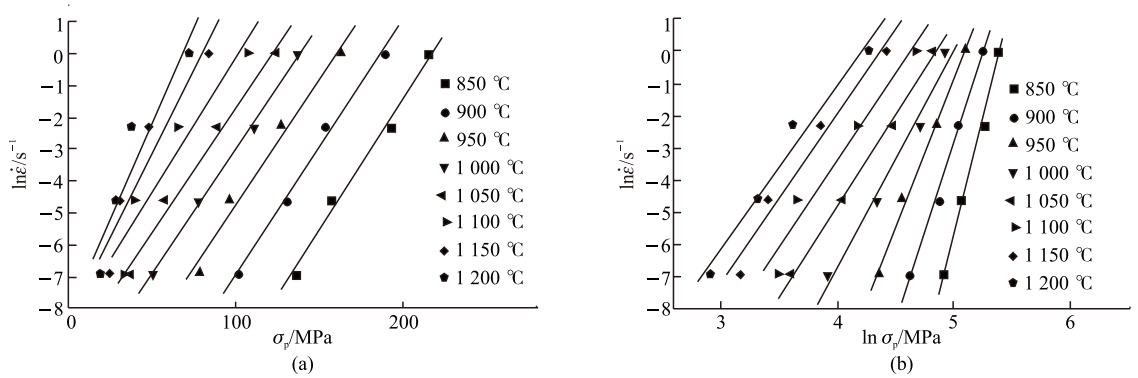

Fig.2 Relationship between lnε̇ and (a) σ; (b) ln(σ) of Nb-added steel

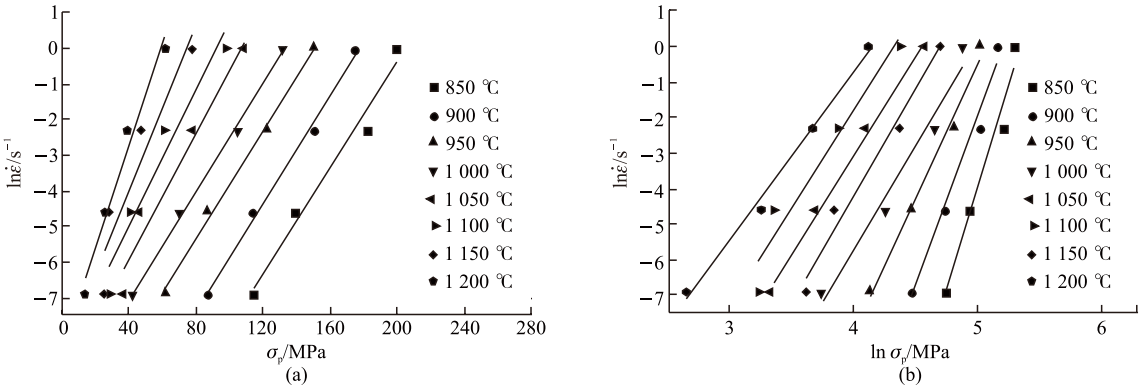

Fig.3 Relationship between lnε̇ and (a) σ; (b) ln(σ) of Nb-free steel

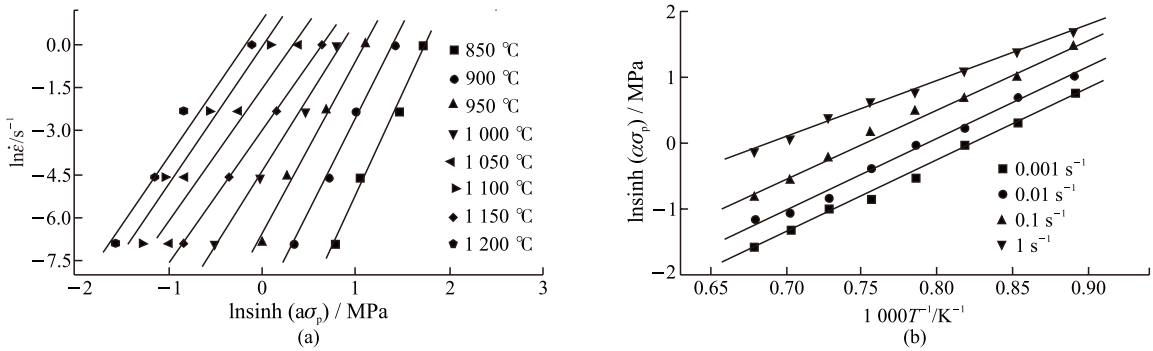

Fig.4 Relationship between (a) lnε̇-lnsinh($\alpha\sigma_p$) and (b) lnsinh($\alpha\sigma_p$)-1 000/T of Nb-added steel

Figs.2(a) and Fig.3(a) are 7.876 3 and 10.922 3, which represent the material constant n of Nb-bearing and Nb-free steel, respectively. Meanwhile, the mean values of all slopes in Fig.2(b) and Fig.3(b) are 0.088 6 and 0.151 0, which represent β of Nb-bearing and Nb-free steel, respectively.Then, the values of α of two test steels are calculated as 0.011 24 MPa^{-1} and 0.013 82 MPa^{-1} for two test steels. If T and $\dot{\varepsilon}$ remain constant, the activation energy Q can be written as:

$$Q = R \cdot \left.\frac{\partial \ln \dot{\varepsilon}}{\partial \ln[\sinh(\alpha\sigma)]}\right|_T \cdot \left.\frac{\partial \ln[\sinh(\alpha\sigma)]}{\partial(1/T)}\right|_{\dot{\varepsilon}} \quad (9)$$

The linear relationships between ln-lnsinh($\alpha\sigma_p$) and lnsinh($\alpha\sigma_p$)-1000/T are shown in Figs.4 (a) and (b) for Nb-added steel and in Figs.5 (a) and (b) for Nb-free steel, respectively. By analyzing the data, the values of apparent activation energy of Nb-bearing and Nb-free steels are determined to be 466 and 406 kJ/mol, respectively. The values of activation energy of test steels are enhanced and the dynamic recrystallizaiton behavior is inhibited due to the addition of Nb. Niobium in solution is the element which most contributes to increasing the activation energy[19]. However, not all the Nb has an influence on the activation energy because some precipitates during hot deformation.

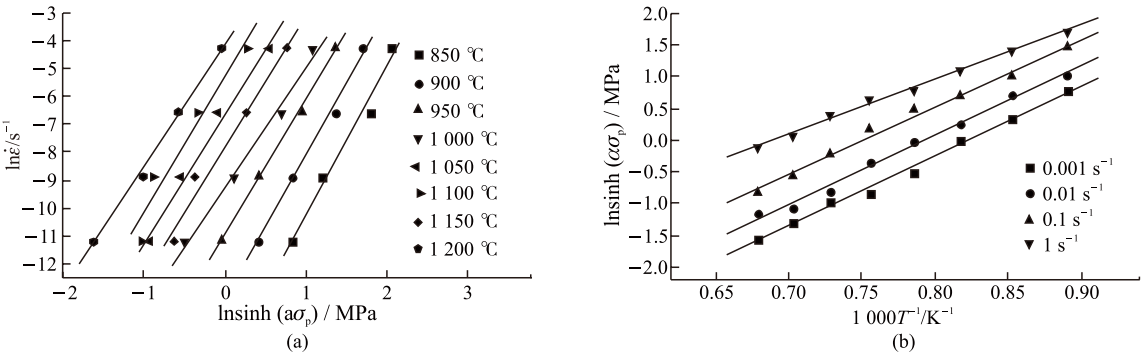

Fig.5 Relationship between (a) ln$\dot{\varepsilon}$-lnsinh($\alpha\sigma_p$) and (b) lnsinh($\alpha\sigma_p$)-1000/T of Nb-free steel

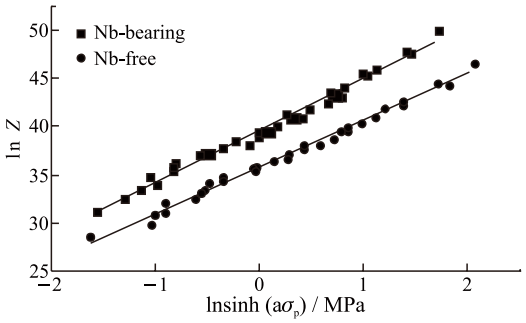

Fig.6 Relationship between ln$Z$ and ln[sinh($\alpha\sigma_p$)]

The relationships between ln$Z$ and ln[sinh($\alpha\sigma_p$)] of two test steels are shown in Fig.6. The correlation factors of the fitted line are 0.974 69 and 0.993 89 and the slope rates are accepted as the values of n, which are 4.368 3 and 4.025 7 for Nb-bearing and Nb-free steels, respectively. The hot deformation equations for two test steels can be expressed as:

$$\dot{\varepsilon}=4.8\times10^{13}[\sinh(\alpha\sigma)]^{4.368\,3}\exp[-466\,000/(RT)] \quad (10)$$

$$\dot{\varepsilon}=2.4\times10^{12}[\sinh(\alpha\sigma)]^{4.025\,7}\exp[-406\,000/(RT)] \quad (11)$$

3.3 Processing maps

On the basis of dynamic material model (DMM) proposed by Prasad and Gegel[23,35], the flow behavior of material undergoing thermoplastic deformation is considered to have the characteristics as dissipative, nonlinear, dynamic, irreversible, and away from equilibrium. DMM theory considers the thermoplastic forming process as the only part of the total processing system and specimen undergoing deformation as a dissipater of power. The instantaneous power P absorbed by the specimen during deformation can be expressed as follows:

$$P=\sigma\cdot\dot{\varepsilon}=G+J=\int_0^{\dot{\varepsilon}}\sigma\cdot\mathrm{d}\dot{\varepsilon}+\int_0^{\sigma}\dot{\varepsilon}\cdot\mathrm{d}\sigma \quad (13)$$

where σ is the flow stress (MPa), $\dot{\varepsilon}$ is the strain rate (s^{-1}), G content and J co-content, which are two complementary parts of P, represent the power dissipated by heat and microstructure evolution, respectively.

The dissipation of power between G and J is controlled by the flow behavior and is defined by a power partitioning factor which is the strain rate sensitivity of flow stress, m:

$$m=\frac{\partial J}{\partial G}=\frac{\partial(\ln\sigma)}{\partial(\ln\dot{\varepsilon})} \quad (14)$$

If the flow stress obeys power law[15]:

$$\sigma=K\dot{\varepsilon}^{\,m} \quad (15)$$

where K is the material constant.

From Eqs.(13) - (15), J is described as follows:

$$J=\int_0^{\sigma}\dot{\varepsilon}\cdot\mathrm{d}\sigma=\frac{\sigma\cdot\dot{\varepsilon}\cdot m}{m+1} \quad (16)$$

For an ideal linear dissipater, m=1 and G=J. Using this definition, the dimensionless efficiency of power dissipation of a non-linear dissipater, η, is expressed as follows:

$$\eta=\frac{J}{J_{\max}}=\frac{2m}{m+1} \quad (17)$$

The variation of η with temperature and strain rate constitutes a power dissipation map. The peak efficiency domains in the power dissipation map may be correlated with the metallurgical processes, *e g*, dynamic recrystallization, dynamic recovery or superplastic deformation. And it can be stated that the optimum hot working condition may occur when η is higher on the premise of no flow instability occurring in this region. The flow instability map is constructed by a continuum instability criterion based on the extreme principles of irreversible thermodynamic applied for

large plastic flow[36], the instability criterion is derived by:

$$\xi\left(\dot{\varepsilon}\right)=\frac{\partial\ln\left(m/m+1\right)}{\partial\ln\dot{\varepsilon}}+m<0 \qquad (18)$$

The variation of ξ may be evaluated as a function of temperature and strain rate to obtain an instability map. The instability regions are characterized as ξ is negative. By superimposing the power dissipation map over the flow instability map in the frame of deformation temperature and logarithm of strain rate, a processing map is eventually established.

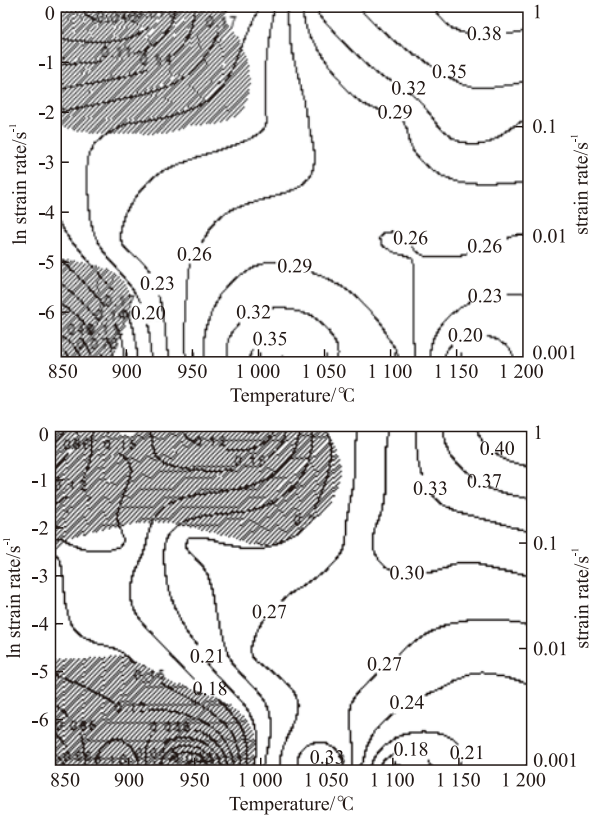

Fig.7 Processing map of two test steels at true strain of 0.7: (a) Nb-free (b) Nb-added

Fig.7 illustrates the processing maps of Nb-free and Nb-bearing steels at true strain of 0.7, which are constructed in the deformation temperatures range of 850 to 1 200 ℃ and strain rates range of 0.001 to 1 s^{-1}. The contour numbers indicate the values of constant efficiency of power dissipation, and the shaded areas represent the instability region where the material exhibits instabilities such as flow localization, adiabatic shear bands or dynamic strain ageing, *etc*. For Nb-free steel, there are two peak domains in the dissipation maps which locate at the temperature ranging from 950 to 1 100 ℃ and strain rate ranging from 0.001 to 0.01 s^{-1}, with an efficiency peak of 35% at 1 000 ℃ and strain rate of 0.001 s^{-1}. And, another peak domain locates at the temperature ranging from 1 025 to 1 200 ℃ and strain rate ranging from 0.01 to 1 s^{-1}, with an efficiency peak of 38% at 1 200 ℃ and strain rate of 1 s^{-1}. The peak domains are in good agreement with Omar's research[37] in medium carbon steel. The two peak domains may be associated with the dynamic recrystallization process which will be confirmed by further microstructural observation. In general, hot deformation process could be conducted in each of these two domains. But the selection of hot deformation parameters should be fit for the industrial manufacture process.

For Nb-bearing steel, there are also two peak efficiency domains in the processing maps. One locates at the temperature ranging from 1 000 - 1 075 ℃ and strain rate ranging from 0.001 to 0.04 s^{-1}, with an efficiency peak of 38% at 1 050 ℃ and strain rate of 0.001 s^{-1}. And another peak domain locates at the temperature ranging from 1 050 - 1 200 ℃ and strain rate ranging from 0.01 to 1 s^{-1}, with a peak efficiency of 42% at 1 200 ℃ and strain rate of 1 s^{-1}. Compared with the non-Nb addition steel, the peak domains of Nb-bearing steel are similar, but the regions move to higher temperature under the same deformation conditions. Nb is the most effective one in retarding the austenite recrystallization by means of the solute drag effect of solution Nb or by pinning effect of strain induced precipitation. The peak domains corresponding to dynamic recrystallization regions move to higher temperature.

It can also be concluded that there are two instability regions for Nb-free steel, one lies in the temperature range from 850 to 1 000 ℃ and strain rate range from 0.1 to 1 s^{-1}, and another lies in the temperature range from 850-900 ℃ and strain rate range from 0.01-0.001 s^{-1}. The instability region of Nb-added steel is similar to that of Nb-free steel, but its regions of instability were larger. In order to obtain desired property after hot rolling process, appropriate parameters for industrial production can be determined according to the processing map and further microstructural observation, which will be discussed in the following content.

3.4 Microstructural evolution and discussion

Fig.8 exhibits the microstructures of two test steels obtained from the peak efficiency domain of processing map, both of which deformed at 1 200 ℃ and strain rates of 1 s^{-1}. The microstructures of two test steels processed in this condition have similar

characteristics with equiaxed and homogeneous grains, which are typical dynamic recrystallized grains. In this region, grain refinement took place by dynamic recrystallization and the workability of material was excellent. The hot deformation processing can be performed in the peak efficiency domain with fully dynamic recrystallization and no flow to obtain desired property. In this condition, there are only a few precipitates existing in the matrix for both test steels, which are shown in Figs.9. (a) and (b). The precipitates are Ti-rich Ti-Nb-V particles in Nb-added steel and Ti-rich Ti-V particles in Nb-free steel, which may be the undissolved particles during reheating. In this condition, most of niobium keeps in solid solution. Hence, the hot deformation behaviors of two test steels were similar while deformed at high temperature in the condition of niobium keeping in s:olid solution.

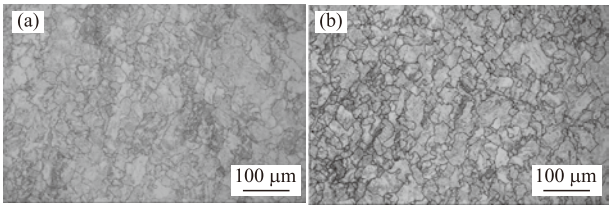

Fig.8 Optical microstructures in the peak efficiency domain of two test steels at a fix strain of 0.7: (a) Nb-added, 1 200 ℃, 1 s^{-1}; (b) Nb-free, 1 200 ℃, 1 s^{-1}

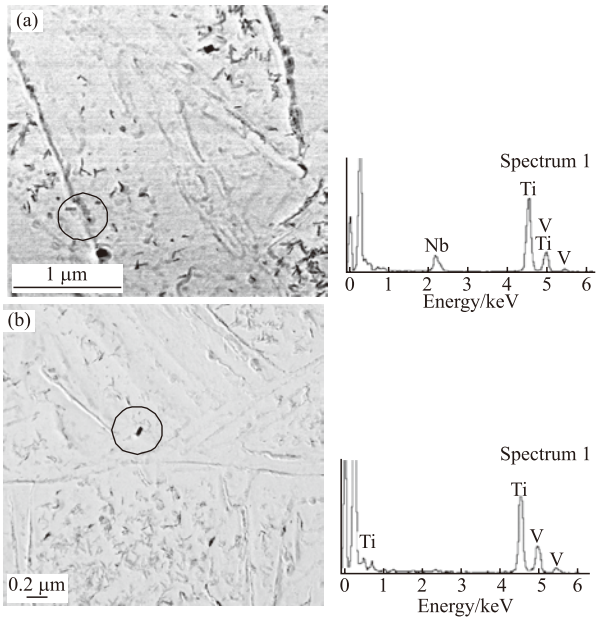

Fig.9 Morphology and energy spectrum of the precipitates deformed at 1 200 ℃ and strain rate of 1 s^{-1}: (a) Nb-added; (b) Nb-free

Figs.10 (a) and (b) are the typical microstructures deformed at peak efficiency domains of relatively low temperature and low strain rate. In this region, fully dynamic recrystallization also took place according to the observation of microstructures. Compared with the microstructure in high temperature domain, the microstructures in this domain exhibit recrystallized grains with wavy boundaries. However, the grains in this region grow quickly with the increase of deformation temperature due to the low strain rate and long deformation time. For Nb-added steel, if the deformation temperature increases from 1 000 to 1 150 ℃, the austenite grain size increases from 29 to 120 μm. Generally speaking, the optimum processing condition is the region with higher efficiency of power dissipation and no instability, where the dynamic recrystallization will be operating to reduce the tendency for flow instability. The hot rolling process of seamless tube seems to be conducted in this region. However, considering the industrial manufacture process[38], the hot-rolling process should be performed at higher temperature and higher strain rate. If conducted in this region, the deformation time is longer than that in higher strain rate domain. So, it is impossible to deform in this region.The microstructures of two test steels obtained from the instability regions are illustrated in Fig.11 and Fig.12, respectively. Two instability regions exist for both test steels in the processing map. When the Nb-added steel deformed at 950 ℃ and strain rate of 0.001 s^{-1}, the grain boundary was flatted and exhibited a few small grains along the grain boundary indicating that there is no fully dynamic recrystallizaiton taking place as shown in Fig.11 (a), whereas the Nb-free steel completed fully dynamic recrystallization under the same deformation condition, which is shown in Fig.10 (b). In this condition, as shown in Figs.13 (a) and (b), the Nb-rich Nb-Ti-V particles precipitated during deformation, and the dynamic recrystallization was inhibited obviously, whereas there was only a little undissolved Ti-rich Ti-V particles existed in Nb-free steel, and the recrystallization process can be completed which is shown in Fig.10 (b). The addition of Nb to the test steel can significantly inhibit dynamic recrystallization, so the suitable deformation temperature was enhanced taken for granted. Microstructures of Nb-bearing steel in this instability region showed diffident feature from those deformed at peak efficiency domains with typical dynamic recrystallization microstructures deformed at 1 000 ℃ and strain rate of 0.001 s^{-1}, which are shown in Fig.10 (a). For Nb-free steel, the typical instability microstructures are shown in Fig.12 (a). Numerous recrystallized grains were formed around the grain boundary indicating the

initial of dynamic recrystallizaiton. In general, grain boundaries are the preferable nucleation sites for dynamic recrystallization[38-41] and the wavy or irregular grain boundaries generally imply the initial stages of DRX. Microstructure observation agrees well with the predictions of processing map. Hot rolling process should not be conducted in this region in case of flow instability during hot deformation. With the increase of deformation temperature, the microstructure could be fully recrystallized, as shown in Fig.10 (b).

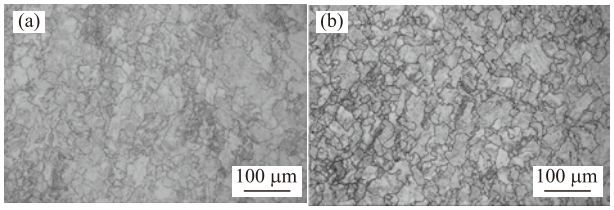

Fig.10 Optical microstructures in the peak efficiency domain of two test steels at strain of 0.7: (a) Nb-added, 1000 ℃, 0.001 s^{-1}; (b) Nb-free, 950 ℃, 0.001 s^{-1}

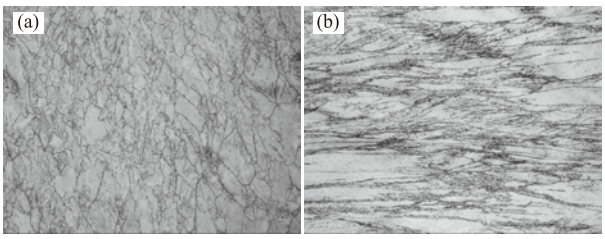

Fig.11 Microstructure observation at strain of 0.7 in the instability region of Nb-added steel: (a) 950 ℃, 0.001 s^{-1}; (b) 950 ℃, 1 s^{-1}

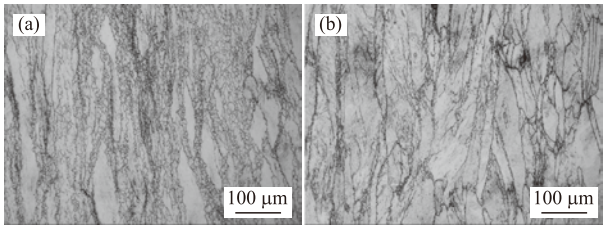

Fig.12. Microstructure observation at strain of 0.7 in the instability region of Nb-free steel: (a) 900 ℃, 0.001 s^{-1}; (b) 950 ℃, 1 s^{-1}

The material of Nb-added steel undergoing instability region of lower temperature and higher strain rate region, *i e*, deformed at 950 ℃ and strain rates of 1 s^{-1}, shows different features from instability regions in lower strain rate region, which is demonstrated in Fig.11 (b). In this region, the material was severely flatted with small recrystallized grains around the grain boundary. A few fine recrystallized grains emerge close to some severe deformation zones which may be correlated with flow instability. At high strain rates, heat generated from the plastic deformation can't escape timely and cause local temperature rising, which could result in adiabatic shear bands or partial dynamic recrystallization. Sivakesavam and Prasad[40] reported that flow localization occurred at lower temperature and higher strain rate. However, cracks and voids were not observed in this condition. But as the strain rate increases further, *i e*, 10 s^{-1} or higher, cracks may be detected due to higher temperature rising in local region and inhomogeneous deformation. Compared with Nb-added steel, the Nb-free steel also experiences uniform deformation, as shown in Fig.12(b). Consequently, the both test steels undergo inhomogeneous deformation in this region which should be avoided during processing.

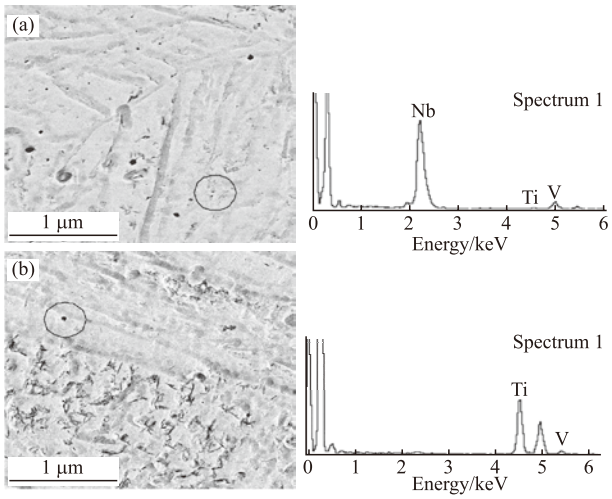

Fig.13 Morphology and energy spectrum of the precipitates deformed at 950 ℃ and strain rate of 0.001 s^{-1}: (a) Nb-added; (b) Nb-free

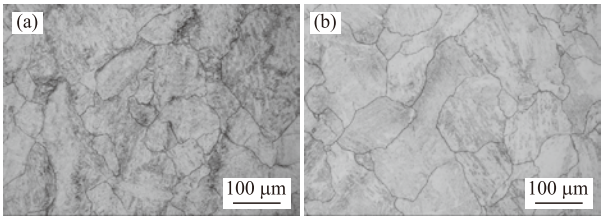

Fig.14 Microstructure observation at a fix strain of 0.7 in the low efficiency domain of two steels: (a) Nb-added, 1 150 ℃, 0.001 s^{-1}; (b) Nb-free, 1 150 ℃, 0.001 s^{-1}

It can be concluded from the processing map that with the increase of deformation temperature and decrease of strain rate, the efficiency of power dissipation increases. But in the region of higher temperature and lower strain rate, a low efficiency domain exists. When both steels deformed at high temperature and low strain rate, *i e*, at 1 150 ℃ and strain rates of 0.001 s^{-1}, abnormal grain growth, as shown in Figs.14 (a) and (b), was observed in this region. The austenite grains grow incessantly and become coarsened easily at high deformation temperature and low strain rate. The coarsened grains

were detrimental to the hot workability of material and the desired property won't be achieved through the following heat treatment. Hence, the hot deformation shouldn't be processed in this region. The research by Cho *et al*[40,41] showed that when the materials deformed at higher temperature and lower strain rates, the martensite microstructures are coarse and the efficiency of dissipation is low. The research is in accord with the results of Nb-added and Nb-free steels in this paper. The reason why the efficiency of dissipation was low is mainly because the energy used for grain growth was much less than the energy dissipated by microstructure transformation. Hence, the efficiency of dissipation was low in this condition compared with that in peak efficiency region. When the material deformed at high temperature and low strain rates, the austenite grains will grow incessantly and the power efficiency by microstructure transformation was relatively low.

4 Conclusions

a) The values of the peak stress and peak strain of Nb-bearing steel were higher than that of Nb-free steel due to the addition of Nb. The values of apparent activation energy of Nb-added and Nb-free are determined to be 466 and 406 kJ/mol, respectively.

b) There are two peak efficiency domains existing in the processing map. Compared with the non-Nb steel, the peak efficiency domains of Nb-bearing steel move to higher temperature due to the inhibition of dynamic recrystallization, and the instability domains of Nb-bearing steel are enlarged due to the precipitation of Nb during deformation.

c) At the high deformation temperature, when most of niobium keeps in solid solution, the hot workability of two test steels was similar. At relatively lower temperature and lower strain rates, niobium precipitated as Nb-rich Nb-Ti-V particles, which make the instability region enlarged.

Acknowledgements

Thanks for the supporting tests of State Key Laboratory of Material Processing and Die & Mould Technology and Analysis and Test Center in Huazhong University of Science and Technology.

References

[1] Meng Fanmao. Application of Niobium, Vanadium and Titanium in Special Steel[J]. *Microalloying Technology*, 2001, 1(1): 28-33

[2] Dong Tao. To Promote the Development and Application of the Microalloying Technology in Our Country[J]. *Microalloying Technology*, 2001,1(1):9-41

[3] Yong Qilong. Physical Metallurgical Data of Niobium in Steel[J]. *Journal of Iron and Steel Research*, 1998, 10(2): 66-69

[4] Yong Qilong, Ma Mingtu. *Micro Alloys - Physical and Mechanical Metallurgy*[M]. Beijing: Mechanical Industry Press, 1989

[5] Dong Tao,Fu Junyan.Physical Metallurgy of Micro Niobium Treated Steel[J]. *Microalloying Technology*, 2002, 2(3): 48-53

[6] Wilmes S, Zwick G. Effect of Niobium and Vanadium as an Alloying Element in Tool Steels with High Chromium Content[C]. *6th International Tooling Conference(Karlstad university)*, 2002

[7] Feng Rui. *Metal Physics*[M]. Beijing: Science Press, 1999

[8] HU Xin-bin,LI Lin,WU Xiao-chun. Application of Niobium Microalloying in Special Steels[J]. *Heat Treatment of Metals*, 2003, 28(6): 5-10

[9] Zhang Shusong, Tong Ailian. *The Toughness Mechanism and Technology Approach of Steel*[M]. Beijing: Weapon Industry Press, 1995

[10] Klaus,V R C Guimarues. Effect of Niobium in Works Steels and Application[J]. *Microalloying Technology*, 2002, 2(2): 49-53

[11] Mercer C and Soboyejo W O. Hall-Petch Relationships in Gamma Titanium Aluminides[J]. *Scripta Materialin*, 1996, 35(1): 17-22

[12] TSUJII N,ABEG.High Temperature Low Cycle Fatigue Behavior of a 4.2Cr-2.5Mo-V-Nb Hot Work Tool Steel[J]. *Journal of Material Science Letters*, 1996, 15: 1 251-1 254

[13] TSUJII N, ABE G. Effect of Testing Atmosphere on Low Cycle Fatigue of Hot Work Tool Steel at Elevated Temperature[J]. *ISIJ. International*, 1995, 35(7): 920-926

[14] Azevedo R, Barbosa E, Pereloma V. Development of Ultrafme Grain Ferrite in Low C-Mn and Nb-Ti Microauyed Steels after Waml Torsion and Intercritical Annealing[J]. *Materials Science and Engineeger A*, 2005, 4(2): 98-108

[15] Cheng L, Chang H, Tang B, *et al*. Deformation and Dynamic Recrystallization Behavior of a High Nb Containing Ti Al Alloy[J]. *Journal of Alloys and Compounds*, 2013, 552: 363-369

[16] Nakashima S,Takashima K,Harase J.Effect of Thickness on Secondary Recrystallization of Fe-3%Si[J]. *Acta Metallurgicalet Materialia*, 1994, 42:539

[17] ZHANG Zhao-hui, LIU Yong-ning, LIANG Xiao-kai, *et al.* The Effect of Nb on Recrystallization Behavior of a Nb Micro-alloyed Steel[J]. *Materials Science and Engineering A*, 2008, 474: 254-260

[18] Sandstrom R, Lagneborg R. A Model for Hot Working Occurring by Recrystallization[J]. *Acta Metallurgica*, 1975, 23(3): 387-398

[19] Rollett AD, Srolovitz DJ, Doherty RD, *et al.* Computer Simulation of Recrystallization in Non-uniformly Deformed Metals[J]. *Acta Metallurgica*, 1989,37(2): 627-639

[20] Gottstein G, Frommert M, Goerdeler M, *et al.* Predicting the Critical Conditions for Dynamic Recrystallization in the Austenitic Steel 800H[J]. *Materials Science and Engineering A*, 2004, 387-389: 604-608

[21] Dehghan-Manshadi A, Barnett M R, Hodgson P D, *et al.* Recrystallization in AISI 304 Austenitic Stainless Steel During and after Hot Deformation[J]. *Materials Science and Engineering A*, 2008, 485: 664-672

[22] Dong L, Zhong Y, Ma Q, *et al*. Dynamic Recrystallization and Grain Growth Behavior of 20SiMn low Carbon Alloy Steel[J]. *Tsinghua Sci. Technol.*, 2008, 13: 609-613

[23] Poliak E I, Jonas J J. A one-parameter Approach to Determining the Critical Condition for the Initiation of Dynamic Recrystallization[J]. *Acta Materialia*, 1996, 44(1): 127-136

[24] Meng Gang,Li Bolong,Li Hongmei, *et al*. Hot Deformation and Proeess-ing Maps Of an Al-5.7wt% Mg Alloy with Erbium[J]. *Materials Science and Engineering A*, 2009, 517(1-2): 132-137

[25] Kyu H O, Jeong J S, Koo Y M, *et al.* The Evolution of the Rolling and Recrystallization Textures in Cold-rolled Al Containing High Mn Austenitic Steels[J]. *Materials Chemistry and Physics*, 2015, 161: 9-18

[26] Xua T C, Peng X D, Qin J, *et al*. Dynamic Recrystallization Behavior of Mg-Li-Al-Nd Duplex Alloy during Hot Compression[J]. *Journal of Alloys and Compounds*, 2015, 639: 79-88

[27] Frost HJ,Ashby MF. *Defomation Mechanism Maps, the Plasticity and Creep Of Metals and Ceramics*[M]. London:Pergamon Press, 1982

[28] Zrink J, Kvackaj T, Sripinproach D, *et al*. Influence of Plastic Deformation Conditions on Structure Evolution in Nb-Ti Microalloyed Steel[J]. *Journal of Material Processing Technilogy*, 2003, 133: 236-242

[29] Liu H, Xue F, Bai J, *et al.* Effect of Heat Treatments on the Microstructure and Mechanical Properties of an Extruded Mg95.5Y3Zn1.5 Alloy[J]. *Materials Science and Engineering: A*, 2013, 585 (0): 261-267

[30] Sivakesavam, Y V R K Prasad. Hot Deformation Behavior of as-cast Mg-2Zn-1Mn Alloy in Compression: a Study with Processing Map[J]. *Materials Science and Engineering A*, 2003, 362(1-2): 118-124

[31] PS Robi, U S Dixit. Application of Neural Networks Ingenerating Processing Map for Hot Working[J]. *Journal of Materials Proeessing Technology*, 2003, 142(l): 289-297

[32] Huang C, Hawbolt EB, Chen X, *et al.* Flow Stress Modeling and Warm Rolling Simulation Behavior of Two Ti-Nb Interstitial-free Steels in the Ferrite Region[J]. *Acta Mater*., 2001 (49): 1 445-1 452

[33] Shukla A K, Narayana Murty S V S, Sharma S C, *et al.* Constitutive Modeling of hot Deformation Behavior of Vacuum hot Pressed Cu-8Cr-4Nb Alloy[J]. *Materials and Design*, 2015, 75: 57-64

[34] Liu XiaoYall, Pan QingLin, He YunBin. Flow Behavior and Microstructural Evolution of Al-Cu-Mg-Ag Alloy During Hot Compression Deformation[J]. *Materials Science and Engineering A*, 2009, 500 (1-2): 150-154

[35] Chen J, Wang Z, Lu S. Effects of Electric Parameters on Microstructure and Properties of Mao Coating Fabricated on ZK60 Mg Alloy in Dual Electrolyte[J]. *Rare Metals*, 2012, 31 (2): 172-177

[36] Xu DK, Han EH. Effects of Icosahedral Phase Formation on the Microstructure and Mechanical Improvement of Mg Alloys: A Review[J]. *Progress in Natural Science: Materials International*, 2012, 22 (5): 364-385

[37] Quan GZ, Li GS, Chen T, *et al*. Dynamic Recrystallization Kinetics of 42CrMo Steel During Compression at Different Temperatures and Strain Rates[J]. *Materials Science and Engineering: A*, 2011, 528 (13-14): 4 643-4 651

[38] Zhu YM, Morton AJ, Nie JF. Growth and Transformation Mechanisms of 18R and 14H in Mg-Y-Zn Alloys[J]. *Acta Materialia*, 2012, 60 (19): 6 562-6 572

[39] Xu SW, Zheng MY, Kamado S, *et al*. Dynamic Microstructural Changes During Hot Extrusion and Mechanical Properties of a Mg-5.0Zn-0.9Y-0.16Zr (wt%) Alloy[J]. *Materials Science and Engineering: A*, 2011, 528 (12): 4 055-4 067

[40] Cho S H, Kang K B, Jonas J J. Mathematical Modeling of the Recrystallization Kinetics of Nb Microalloyed Steels[J]. *ISIJ International*, 2001, 41 (7): 766-773

[41] Vervynck S, Verbeken K, Thibaux P, *et al*. Recrystallization-precipitation Interaction during Austenite Hot Deformation of a Nb Microalloyed Steel Mater[J]. *Materials Science and Engineering A*, 2011, 528: 5 519-5 528